reverses the helicity of the polarization), but μ_L (here either HV/HH or VH/VV) is close to zero (*9*). Surface scattering from surfaces of root mean square height comparable to or larger than the radar wavelength, such as rough lava flows [J. J. van Zyl, C. F. Burnette, T. G. Farr, *Geophys. Res. Lett.* **18**, 1787 (1991)], yields $\sigma^0_{RL} < 0.2$, $\mu_C < 0.4$, and $\mu_L < 0.2$ at all three wavelengths, for $\theta = 30°$. Volume scattering from heavily vegetated areas, such as tropical rain forest [A. Freeman, S. Durden, R. Zimmerman, in *Proceedings of the International Geoscience and Remote Sensing Symposium, Houston, Texas, May 26–29, 1992*, R. Williamson, Ed. (IEEE, New York, 1992), p. 1686] yields $\mu_C \approx 1$ and $\mu_L \approx 0.3$ at 24 and 68 cm, $\mu_C \approx 0.8$ and $\mu_L \approx 0.25$ at 5.6 cm, but $\sigma^0_{RL} < 0.1$ at all three wavelengths, for $\theta = 55°$. Unlike Greenland, none of these objects show very strong echoes with large polarization ratios.

12. D. B. Campbell, R. A. Simpson, S. J. Ostro, unpublished data.
13. H. J. Zwally, *J. Glaciol.* **18**, 195 (1977).
14. C. T. Swift, P. S. Hays, J. S. Herd, W. L. Jones, V. E. Delmore, *J. Geophys. Res.* **90**, 1983 (1985).
15. B. Hapke, *Icarus* **88**, 407 (1990).
16. F. C. MacKintosh and S. John, *Phys. Rev. B* **37**, 1884 (1988); M. P. van Albada, M. B. van der Mark, A. Lagendijk, in *Scattering and Localization of Classical Waves in Random Media*, P. Sheng, Ed. (World Scientific, Singapore, 1990), p. 97, and references therein.
17. K. J. Peters, *Phys. Rev. B* **46**, 801 (1992).
18. M. I. Mishchenko, *Earth Moon Planets* **58**, 127 (1992).
19. S. J. Ostro and E. M. Shoemaker, *Icarus* **85**, 335 (1990). In contrast to the case of Ganymede and Callisto, few impact craters have been identified on Europa, and it is not clear whether the surficial layer of Europa is generated primarily by impacts or by internal processes, such as frost deposition.
20. We thank R. Thomas, head of the Polar Research Program at NASA Headquarters, for supporting this research; the people from the AIRSAR team for collecting and processing the SAR data used in this manuscript; J. Crawford for coordinating the AIRSAR overflights; and P. Gogineni and M. Drinkwater for discussions about Greenland glaciology. Part of this work was carried out at the Jet Propulsion Laboratory, California Institute of Technology, under contract with NASA.

28 April 1993; accepted 2 August 1993

Evidence for a Low Surface Temperature on Pluto from Millimeter-Wave Thermal Emission Measurements

S. Alan Stern,* David A. Weintraub, Michel C. Festou

Thermal continuum emission from the Pluto-Charon system has been detected at wavelengths of 800 and 1300 micrometers, and significant upper limits have been obtained at 450 and 1100 micrometers. After the subtraction of emission from Charon, the deduced surface temperature of much of Pluto is between 30 and 44 kelvin, probably near 35 to 37 kelvin. This range is significantly cooler than what radiative equilibrium models have suggested and cooler than the surface temperature derived by the Infrared Astronomy Satellite. The low temperature indicates that methane cannot be present at the microbar pressure levels indicated by the 1988 stellar occultation measurements and that the methane features in Pluto's spectrum are from solid, not gas-phase, absorptions. This result is evidence that Pluto's atmosphere is dominated by nitrogen or carbon monoxide rather than methane.

Because of Pluto and Charon's large distance from the Earth and the small sizes of these two bodies, studies of the Pluto-Charon system (PCS) are difficult (*1*). A number of fundamental issues in the PCS remain unresolved, such as Pluto's temperature, its bulk atmospheric composition, and the validity of its oft-cited analogous relationship to Triton. To improve the constraints on these and other important issues, we have undertaken a program of submillimeter measurements of the thermal emission from the PCS. Previous PCS thermal detections have been reported at wavelengths of 60, 100, and 1300 μm; however, these results are discrepant (*2*, *3*).

Our measurements were made in 1991 and 1993. The 1991 measurements were made at an effective wavelength of 1100 μm on 8 October UT with the UKT14 bolometer at the Nasmyth focus of the 15-m James Clerk Maxwell Telescope (JCMT) on Mauna Kea, Hawaii (*4*). The 1993 measurements were made at effective wavelengths of 450, 800, 1100, and 1300 μm on 26 January UT with the same instrument, and again at 1300 μm on 19 February UT with the MPIfR seven-channel bolometer on the 30-m Institut de Radio Astronomie Millimétrique (IRAM) telescope at Pico Veleta, Spain.

The UKT14 (*5*) is a sensitive ^{3}He-cooled, single-channel bolometer with a filter wheel and variable iris. The observations reported here were made with the instrument's 65-mm-diameter circular diaphragm fully open. Sky cancellation was achieved with a chopping secondary set to make both 40–arc sec and 60–arc sec east-west chops at a frequency of 7.8 Hz. The wavelength-dependent, half-power beam widths (HPBWs) for fully open diaphragm observations with UKT14 are given in Table 1. The MPIfR bolometer (*6*) is conceptually similar to the UKT14 instrument but offers the advantage of seven spatial elements arranged in a six-element daisy pattern around the central channel. Each beam has an HPBW of 12 arc sec at 1300 μm. At IRAM, the sky-chopping secondary was set to an east-west throw of 45 arc sec at a frequency of 2.0 Hz.

Accurate pointing for each observation was determined by offsetting to the calculated PCS position (*7*) after the use of a Gaussian fit routine to center on bright, nearby millimeter point sources. The telescope pointing errors derived from pointing checks on these nearby sources were 1 to 2 arc sec root mean square; these are small compared to the telescope beam size.

Uranus was used to calibrate the measured flux density for the 1991 JCMT and 1993 IRAM observations. Jupiter was used to calibrate the 1993 JCMT observations. We used the standard submillimeter telescope correction algorithm to compensate for finite-size effects of Uranus and Jupiter in the telescope beam. We adopted brightness temperatures for Uranus of 92.5 and 97.5 K at 1100 and 1300 μm, respectively. For Jupiter we adopted brightness temperatures of 148.5, 162.5, 170, and 170 K at 450, 800, 1100, and 1300 μm, respectively. We performed additional checks on the flux calibration and on the variability of the atmospheric optical depth at JCMT by observing several secondary calibrators [W3(OH), CRL 2688, CRL 618, and NGC 7538 IRS1, and 16293-2422] during the night at several times (*8*). At IRAM, telescope elevation scans called sky dips were routinely made to characterize the telluric opacity. The 1300-μm zenith opacities for our observing sessions are given in Table 1.

The maximum angular separation between Pluto and Charon is only 0.9 arc sec; hence our measurements represent the combined flux density from both Pluto and Charon (Table 1). Figure 1A depicts this set of measurements, along with Altenhoff and colleagues' 1300-μm grand average of 15 ± 1.4 mJy made in 1986. The January and February 1993 observations were of the same hemisphere of Pluto. The combination of our multiple observations gives an error-weighted detection of 10.5 ± 5.1 mJy at 1300 μm. At 800 μm we detected 33 ± 7 mJy from the PCS.

To invert our measurements and derive a temperature solution for Pluto, we first write the total flux density from Pluto and Charon as the superposition of the flux from their two gray-body Planck functions

S. A. Stern, Space Sciences Department, Southwest Research Institute, 6220 Culebra Road, San Antonio, TX 78238.
D. A. Weintraub, Department of Physics and Astronomy, Vanderbilt University, Nashville, TN 37235.
M. C. Festou, Observatoire Midi-Pyrénées, F-31400 Toulouse, France.
*To whom correspondence should be addressed.

$$F(\nu) = \epsilon_{ch}\left(\frac{R_{ch}}{\Delta}\right)^2 B_\nu(\overline{T}_{ch}) + \epsilon_{pl}\left(\frac{R_{pl}}{\Delta}\right)^2 B_\nu(\overline{T}_{pl}) \quad (1)$$

where pl represents Pluto, ch represents Charon, ν is the frequency of the observation, $\overline{T}$ is the body's average temperature, ϵ is the body's submillimeter surface emissivity (assumed to be wavelength-independent), R is the body's radius, Δ is the geocentric distance of the PCS, and $B_\nu(\overline{T})$ is the Planck function, evaluated at temperature $\overline{T}$. When Eq. 1 is evaluated, the temperatures of Pluto and Charon must be handled differently. For Pluto, one uses a single (that is, position-independent) $\overline{T}_{pl}$ because Pluto's surface temperature is assumed to be globally regulated to a single isothermal value by latent heat exchange from sublimating volatile ices of N_2, CO, and CH_4 (9). However, Charon's surface consists of H_2O, which cannot sublimate and globally regulate the surface temperature at 30 astronomical units (AU). For that reason, Charon's surface temperature is not globally constant and must be represented by a model that allows for cosine-loss insolation effects with subsolar latitude.

To derive the surface temperature of Charon, we use the standard thermal model for outer solar system satellites (*10*), the isothermal latitude model. According to this model, at any given subsolar latitude Λ

$$T_{ch}(\Lambda) = \left(\frac{F_\odot(1-A)\cos\Lambda}{\pi\sigma\beta\bar{\epsilon}_{IR}D^2}\right)^{1/4} \quad (2)$$

where $F_\odot$ is the solar constant at 1 AU, D is the heliocentric distance of Charon in astronomical units, A is Charon's spherical albedo, σ is Stefan's constant, $\bar{\epsilon}_{IR}$ is Charon's average surface infrared (IR) emissivity, and β is Charon's IR beaming (that is, emission asymmetry) factor (*10*). On the basis of Charon's visible albedo and the phase integrals of the most likely analog objects, the icy Uranian satellites (*10*), we adopt $A = 0.18$, with an estimated error of 20%. On the basis of data for typical icy satellites, we also adopt $\bar{\epsilon}_{IR} = 0.90$ and $\beta = 0.8$ (*2*, *10*). These parameters give a T_{ch} ($\Lambda = 0$) of 55 K. Even if β and $\bar{\epsilon}_{IR}$ vary over the plausible ranges of $0.7 < \beta < 0.8$ and $0.8 < \bar{\epsilon}_{IR} < 1.0$ (*11*), T_{ch} ($\Lambda = 0$) is constrained between 54.7 K and 59.8 K. Even if $\beta = 1$, T_{ch} ($\Lambda = 0$) would only fall to 51.7 K. These results indicate that Charon's surface temperature is both warm (in this context) and relatively well constrained by the available input parameters. This temperature range is in agreement with previous Charon model results (*2*).

To obtain global average temperature $\overline{T}_{ch}$ we average over Λ and the azimuth angle around the subsolar point ϕ as follows

$$\overline{T}_{ch} = \frac{\int T(\Lambda,\phi)d\Omega}{\int d\Omega} \quad (3)$$

Where ϕ represents longitude, the integration is performed over the hemisphere visible from Earth, and

$$d\Omega = \frac{2\pi R^2_{ch}}{\Delta^2}\sin\Lambda\cdot\cos\Lambda d\Lambda \quad (4)$$

With $\overline{T}_{ch}$, we remove Charon's contribution from the total flux density in Eq. 1 to give a Pluto-only flux density dependent solely on R_{pl}, $\overline{T}_{pl}$, and ϵ_{pl}.

We have plotted the Pluto-only flux distribution (Fig. 1B) by removing the Charon contribution to the PCS flux density at each wavelength. In doing so, we assumed an R_{ch} of 620 km (*1*, *12*). Charon's contribution amounts to 30 to 38% of the total PCS flux in the submillimeter-millimeter wavelength regime. Figure 1B also shows a weighted least-squares fit to the long-wavelength (that is, Rayleigh-Jeans) portion of the Planck function; this fit is made with the four detections of Pluto at 800 μm and 1300 μm and their respective error bars (Table 1). At least in this long-wavelength region, the good quality of the fit indicates there is no systematic wavelength dependence of Pluto's emissivity for $800 \leq \lambda \leq 1300$ μm.

In Fig. 2 we depict data from the net Pluto-only flux density derived from the JCMT and IRAM measurements, as well as the net Pluto-only IRAS fluxes reported by Sykes and colleagues and Tedesco and coworkers (*2*), adjusted for geocentric distance to the 1993.1 epoch. We also plot a set of Planck curves giving Pluto's flux density measured from the Earth during 1993.1 as a function of its isothermal surface temperature. The Planck curves in Fig. 2, A and B, were computed on the assumption of constant emissivities of 1.0 and 0.7, respectively, and an R_{pl} of 1180 km (*1*, *12*).

The JCMT and IRAM data points clearly indicate a surface-temperature solution in the range of 30 to 35 K if Pluto's surface emissivity is near unity. However, because the three ices that have been detected on Pluto's surface, CH_4, CO, and N_2 (*13*) have low molecular polarizabilities, a surface emissivity somewhat below unity is likely. A plausible emissivity for these ices is 0.7 (9). With the adoption of this emissivity, our data and the model described above indicate a higher surface temperature of 38 to 44 K (*14*). Taking the full range of temperatures consistent with $0.7 < \epsilon_{pl} < 1$, we find that our data indicate surface temperatures in the range of 30 to 44 K.

The IRAS and JCMT-IRAM data sets fall on significantly different curves for any

Table 1. Submillimeter-millimeter thermal emission measurements of the PCS from 1991 to 1993. All measurements below were taken with the JCMT except those for 1993 Feb. 19.4. Upper limits are given at 3σ confidence. New measurements at 1300 μm (*23*) confirm the results presented here.

Date (UT)	λ (μm)	HPBW (arc sec)	Zenith opacity (1300 μm)	Flux density (mJy)
1993 Jan. 26.8	0450	17.5	0.03	<151
1993 Jan. 26.8	0800	16.8	0.03	33 ± 07
1991 Oct. 08.2	1100	18.5	0.18	<36
1993 Jan. 26.8	1100	18.5	0.03	<24
1993 Jan. 26.8	1300	19.5	0.03	12 ± 10
1993 Feb. 19.4	1300	12.0	0.12	10 ± 06

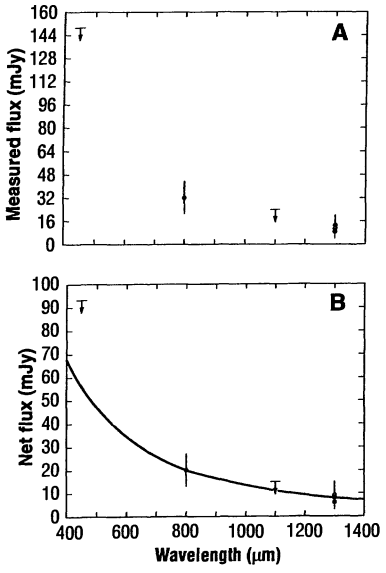

Fig. 1. (**A**) The full set of available submillimeter-millimeter PCS flux measurements and upper limits (arrows) [in millijanskys (mJy)]. The plotted value for the 1986 measurement of Altenhoff and co-workers (*3*) was corrected for Pluto's geocentric distance from 1986.2 to 1993.1 to place it on an equivalent basis with the later measurements; the Altenhoff measurement is the uppermost 1300-μm point. All other measurements were made in 1991 and 1993. (**B**) The same data are shown after subtraction of Charon's flux, determined from a blackbody solution with R_{ch} = 620 km, T = 57.5 K, ϵ = 0.9, and the standard 1993.1 observing geometry described in the text. The overplotted line is a weighted Rayleigh-Jeans fit to the 800- and 1300-μm Pluto-only fluxes (T = 35 K).

wavelength-independent surface emissivity (Fig. 2), which leads to a second finding: The temperature envelope derived from the submillimeter-millimeter measurements is not a priori compatible with the IRAS data published by Sykes and co-workers. Indeed, our measurements and model results significantly exacerbate the discrepancy between long-wavelength IR and submillimeter measurements noted some years ago (*2*).

The cold temperature (30 to 44 K) JCMT-IRAM solution is preferable to the warmer (55 to 60 K) solution obtained from IRAS data because the cold temperature range is compatible with the near-surface pressure derived from the 1988 stellar occultation. This pressure constraint is in the range of 1 to 3 microbars (*1*, *15*). We combined this constraint in Fig. 3 with the calculated vapor pressure curves of the three spectroscopically detected volatiles on Pluto's surface: CH_4, CO, and N_2. The cold temperatures indicated by the JCMT and IRAM data fit well with an N_2- or CO-dominated atmosphere with a surface pressure in the occultation constraint range. By contrast, the previously published warm Infrared Astronomy Satellite (IRAS) solution is incompatible with the occultation data (*16*).

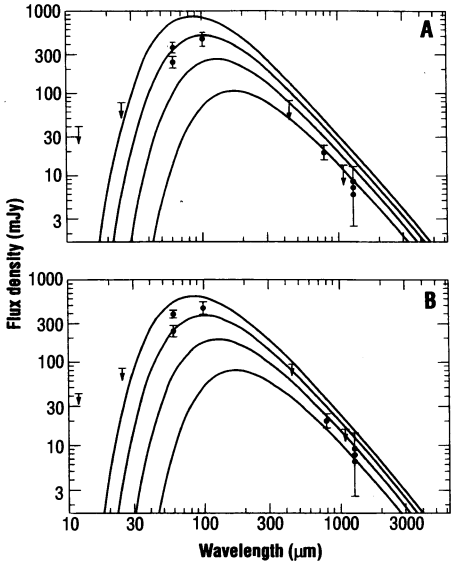

Fig. 2. Data from this study, the 1986 Altenhoff measurements (*3*), and the various 12-, 25-, 60-, and 100-μm IRAS results (*2*) obtained in 1983 are depicted against a suite of increasing Planck function curves with surface temperatures on Pluto of 30, 40, 50, and 60 K, respectively. All of these measurements have been reduced to the common 1993.1 observing circumstances described in the text and have had the model Charon contribution removed. (**A**) Blackbody curves for $\epsilon_{pl} = 1$. (**B**) Blackbody curves for $\epsilon_{pl} = 0.70$. At 60 μm, the IRAS obtained an upper limit in the sky survey observations and a detection in pointed observations (*2*).

How might the IRAS and JCMT-IRAM data sets be reconciled? Alternatives include: (i) a dramatic cooling of Pluto between the 1983 IRAS measurements and the 1988 occultation; (ii) the possibility that the IRAS object identified as the PCS is either some distant background source or the PCS superimposed on a background source; (iii) a wavelength-dependent surface emissivity; and (iv) a nonisothermal Pluto (that is, with hot spots of "bare" ground devoid of sublimating ices) (*17*).

We strongly discount any possibility of a dramatic cooling between 1983 and 1988 because Pluto drew closer to the sun and because visible-wavelength photometric observations have not revealed any thermally significant albedo change. Because Sykes and co-workers carefully checked their data for the possibility of background sources, we also discount that possibility. Instead, we prefer either a wavelength-dependent surface emissivity or, more likely, a nonisothermal surface that contains both cold (volatile-sublimating) and warmer (sublimation-free) units. The fact that the data presented in Fig. 1 are so well represented by a constant-emissivity Rayleigh-Jeans fit encourages the conclusion that a two-temperature surface model is the more viable hypothesis.

Additional data are required to determine whether the flux discrepancy between the 60- to 100-μm and fluxes is due to wavelength-dependent emissivities or to a combination of hot and cold surface units. To this end we have begun a program both to extend the set of submillimeter measurements to shorter wavelengths and to obtain a rotationally resolved set of high submillimeter and millimeter signal-to-noise, wavelength light curves of the PCS. If there are both cold and warm surface units, then the thermal light curve should be anticorrelated with its albedo light curve.

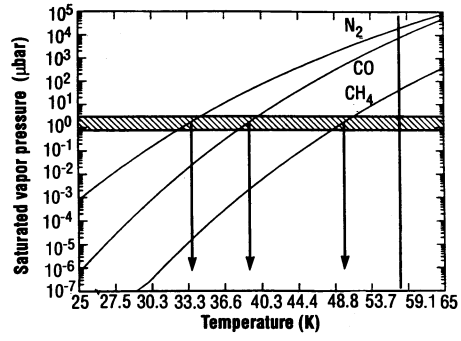

Fig. 3. The vapor pressure equilibrium curves for N_2, CO, and CH_4 ices as a function of temperature (indicated by arrows) (*22*). The occultation-derived, near-surface pressure constraints for Pluto's atmosphere (*15*) are depicted by the hatched area between the solid horizontal lines. The horizontal line furthest to the right represents the IRAS temperature of Sykes and colleagues in (*2*).

The implications of the cold Pluto surfaces indicated by our data are far-reaching. First is the strong evidence provided for an N_2- or CO-, rather than CH_4-, dominated atmosphere (Fig. 3). At the relative vapor pressures of N_2, CO, and CH_4 shown in Fig. 3, CH_4 is expected to be present in the atmosphere only as a minor (if not trace) constituent. Second, if CH_4 is present in the atmosphere at the column abundance indicated by the cold surface result ($\ll$1 cm·am), then the atmospheric column is not sufficient (*18*) to produce the strong CH_4 bands long seen in Pluto's spectrum (*1*). Instead, these bands must be formed by solid-state absorptions in the surface CH_4 frosts, resolving the question of how Pluto's tenuous atmosphere could produce the visible-wavelength CH_4 bands (*19*). The third implication of the cold surface temperature can be derived from a simple radiative balance calculation. Using such a model, we find that Pluto's spherical albedo, *A*, must be in the range of 0.66 to 0.89. Because *A* is formally defined as the product of the geometric albedo *p* and a phase integral *q* (*20*), Pluto's mean visible geometric albedo of 0.51 (*21*) indicates that, for this planet, $1.2 < q < 1.8$. Finally, as a relevant comparison, Neptune's satellite Triton and Pluto have similar sizes, bulk densities, surface compositions, and locations in the solar system (*1*). The evidence presented here for a Pluto with cold, volatile-subliming surface units, an N_2- or CO-dominated atmosphere, and a phase integral >1 suggests that Pluto and Triton are similar in these important respects as well. However, if Pluto is found to exhibit both cold and warm surface units (Triton does not), then an important difference between these two complex bodies will have been established.

REFERENCES AND NOTES

1. S. A. Stern, *Annu. Rev. Astron. Astrophys.* **30**, 185 (1992).
2. Pointed Infrared Astronomy Satellite (IRAS) observations were reported and analyzed by M. V. Sykes, R. M. Cutri, L. A. Lebofsky, and R. P. Binzel [*Science* **237**, 1336 (1987)]. Lower signal-to-noise sky survey observations were reported and analyzed by E. Tedesco, G. Veeder, R. Dunbar, and L. Lebofsky [*Nature* **327**, 127 (1987)].
3. Before our work, the IRAS data and high-temperature interpretation published by Sykes and colleagues was widely accepted, but there was the nagging issue of Altenhoff's single millimeter-wavelength measurement, with its low-temperature connotation. This observation had not been confirmed, and doubts had been expressed about the ephemeris used to point at Pluto and the fact that his measurements had been made at a single wavelength. Our work demonstrates that the IRAS result is at odds with a comprehensive submillimeter-millimeter data set, including the work of W. J. Altenhoff and co-workers [*Astron. Astrophys.* **190**, L15 (1988)]. Although this report of Altenhoff and colleagues cites measurements at 1200 μm (250 GHz), R. Chini, a co-author,

informs us (personal communication) that these measurements were actually made at 1300 μm (236 GHz).
4. The JCMT is operated jointly by the United Kingdom Science and Engineering Research Council, the Netherlands Organizations for the Advancement of Pure Research, the Canadian National Research Council, and the University of Hawaii.
5. W. D. Duncan, E. I. Robson, P. A. R. Ade, M. J. Griffin, G. Sandell, *Mon. Not. R. Astron. Soc.* **243**, 126 (1990).
6. E. Kreysa, R. Lemke, C. G. T. Haslam, A. W. Sievers, *Astron. Astrophys. Lett.*, in press.
7. The positions of the PCS were determined from ephemerides in the *Astronomical Almanac for the Year 1993* (Government Printing Office, Washington, DC, 1993).
8. Our pointing sources were taken from a recent submillimeter catalog [G. Sandell, in preparation]. The Uranus and Jupiter calibration measurements are referenced from the work of M. J. Griffin and co-workers [*Icarus* **65**, 244 (1986)] and G. S. Orton and colleagues [*ibid.* **67**, 289 (1986)].
9. L. M. Trafton and S. A. Stern. *Astrophys. J.* **267**, 872 (1983).
10. L. A. Lebofsky and J. R. Spencer, in *Asteroids II*, R. P. Binzel, T. Gehrels, M. S. Matthews, Eds. (Univ. of Arizona Press, Tucson, 1990), pp. 128–146.
11. Estimates of the vertical scale length of the diurnal thermal wave on Pluto are between 50 and 1000 times the wavelength of our measurements (*1, 9*). Because these values are thick compared to the ~10 wavelength penetration of common dielectrics in the millimeter wave regime [B. L. Ulich, J. R. Dickel, I. De Pater, *Icarus* **60**, 590 (1984)], it is reasonable to conclude that our measurements sample the thermally relevant skin temperature.
12. The radius of Charon is known to lie between 600 km and 640 km (*1*). The 620-km value used here is intermediate and can introduce no more than a 6% error in Charon's flux contribution, corresponding to no more than 1 to 2% of the total PCS flux. The radius of Pluto is uncertain at the ±3% level, owing to discrepancies between mutual event and stellar occultation data (*1*). The range of solutions falls between 1151 km and 1220 km. A radius of 1180 km is a conservatively small value, on the basis of the most complete analysis [R. L. Millis *et al.*, unpublished data].
13. T. Owen *et al.*, *Science* **261**, 745 (1993).
14. If either Pluto or Charon has a radius at its upper limit (642 and 1220 km, respectively), as opposed to the 1180- and 620-km values used above, solutions up to 3 to 4 K colder would be indicated. Similarly if Pluto or Charon had a radius at its lower limit (602 and 1151 km, respectively), then solutions 2 to 3 K warmer would be indicated. If the surface emissivity on Pluto is as low as 0.5, the surface temperature would be driven into the 55- to 60-K range of the IRAS-derived results. However, this temperature is not consistent with pressure data on Pluto's atmosphere (*15*).
15. J. L. Elliot and L. A. Young, *Astron. J.* **103**, 991 (1991).
16. If Pluto is cold (30 to 43 K) and Charon is warm (53 to 59 K) as predicted by our model, then the PCS would have been below the IRAS detection limits.
17. It is also possible that there is some contribution from a rotationally variable thermal flux from Charon.
18. The total column abundance (N_{tot}) is derived from the total pressure, with the use of the perfect gas law and the scale height measured during the 1988 occultation, giving $N_{tot} = 0.6 \times 10^{15}$ to 1.8×10^{15} cm^{-2}. The small CH_4 mixing ratio suggested by the low surface temperature may be at odds with the popular methane-induced atmospheric thermal gradient model [R. V. Yelle and J. I. Lunine, *Nature* **339**, 288 (1989)].
19. On the basis of laboratory data, the visible-wavelength CH_4 bands on Pluto appeared to require a much higher atmospheric column than those that early thermal models indicated were present (*1*). This problem motivated some early suggestions (*9*) for a very low emissivity, high-temperature surface that would support a relatively dense atmosphere (compared to the established, 1- to 3-μbar pressure). The cold Pluto results found here bolster previous evidence [M. W. Buie and U. Fink, *Icarus* **70**, 483 (1987)] concerning this old quandry by demonstrating that the visible-wavelength CH_4 absorptions must be formed by the solid-state frost rather than by an overlying gas column.
20. The spherical albedo, A, is the ratio of total radiative flux emitted by a spherical object in all directions to the incident flux on it. By definition, $A = pq$, where p is the geometric albedo and q is the so-called phase integral. The geometric albedo is the ratio of the brightness of an object to that of a perfectly diffusing disk of the same size, under the same illumination conditions. The phase integral is a numerical coefficient describing the integral behavior of the object's phase function over its surface.
21. The range of 0.44 to 0.59 in Pluto's geometric albedo [D. J. Tholen and M. W. Buie, *Astron. J.* **96**, 1977 (1989)] is dominated by Pluto's 25% light-curve amplitude and uncertainties in Pluto's radius; strict measurement errors are less than 1%.
22. Accurate polynomial fits to laboratory vapor pressure data taken over a number of cosmogonically important ices at temperatures of 30 to 80 K are given by G. N. Brown, Jr., and W. T. Ziegler [*Advances in Cryogenic Engineering* (Plenum, New York, vol. 25, 1980), p. 662].
23. We obtained additional JCMT observations of Pluto and Charon on 22 May 1993 UT with significantly improved observation times yield 15 ± 4.8 mJy at 1300 μm. This value confirms our previous results.
24. We thank the staffs of the JCMT and IRAM observatories for their assistance with the observations and M. Buie, I. De Pater, L. Lebofsky, J. Spencer, M. Sykes, and D. Tholen for useful discussions.

10 May 1993; accepted 16 July 1993

The Origin of the Turtle Body Plan: Bridging a Famous Morphological Gap

Michael S. Y. Lee

A restudy of pareiasaurs reveals that these primitive reptiles are the nearest relatives of turtles. The two groups share numerous derived characters, such as a reduced presacral count, an acromion process, and a trochanter major, which are absent in other basal amniotes. Many traits long thought specific to chelonians also occur in pareiasaurs and must have evolved before the distinctive turtle shell appeared. Evidence uniting captorhinid or procolophonoids with turtles is shown to be weak. The phylogeny proposed here also suggests that certain features of the earliest turtle (*Proganochelys*) that have been interpreted as specializations, such as the large supratemporal and robust metacarpals, are primitive for turtles. In pareiasaurs, the osteoderms represent the precursors of the chelonian shell and the morphology of the anterior region is consistent with the idea that the shoulder girdle in turtles has migrated posteriorly into the rib cage.

Turtles, mammals, and birds differ greatly from their primitive reptilian ancestors. However, although the mammal and bird origins are both documented by numerous transitional fossils, turtles appear abruptly. Distinctive chelonian features such as the carapace, plastron, and the location of the shoulder girdle within the rib cage are already well developed in the earliest known turtles (*1*). Attempts by morphologists to understand how the turtle body plan arose have been hindered by the apparent absence of intermediate forms (*2*). In this report, I demonstrate that pareiasaurs are the closest relatives of turtles and are intermediates between turtles and generalized reptiles.

Pareiasaurs (*3*) are large anapsid reptiles that flourished briefly and achieved a cosmopolitan distribution during the Late Permian (*4*). These ponderous, heavily armored herbivores appear to form a monophyletic group, characterized by several derived traits such as crenulated ("iguanodont") teeth, large descending cheek flanges that cover the posterior region of the lower jaw, a prominent ventral boss on the mandible, four or more sacral vertebrae, a forwardly directed ilium, a reduced pubis, and a wide, flattened femoral shaft. Because new information from a thorough reexamination of these poorly known creatures was expected to shed light on their relations with other reptiles, a cladistic analysis of pareiasaurs and other basal amniotes was undertaken (*5*).

Pareiasaurs were found to share 16 derived features with turtles (Figs. 1 to 4): (A1) a choana located far medially from the alveolar ridge of the maxilla, largely separating the palatine from the vomer; (A2) a large, circular, medially located foramen palatinum posterius (the suborbital foramen of diapsids is more laterally located and of a different shape); (A3) a massive horizontal paroccipital process firmly sutured to the squamosal (also sutured to the supratemporal in pareiasaurs and to the quadrate in turtles); (A4) a long lateral flange of the exoccipital on the posterior face of the paroccipital process; (A5) a basisphenoid and basioccipital solidly ossified together, resulting in the loss of the ventral otic fissure that

University Museum of Zoology, Downing Street, Cambridge CB2 3EJ, United Kingdom.